Arbitrary Termination Impedances, Arbitrary Power Division, and Small-Sized Ring Hybrids

Hee-Ran Ahn, *Member, IEEE,* Ingo Wolff, *Fellow, IEEE,* and Ik-Soo Chang, *Member, IEEE*

***Abstract*— If a ring hybrid is terminated by arbitrary impedances, design equations cannot be derived with conventional methods because symmetry planes for even- and/or odd-mode excitation are not available. Therefore, under these conditions, new design equations for ring hybrids were derived. They can be applied to ring hybrids with both arbitrary termination impedances and arbitrary power-division ratios. Also, new design equations for small-sized ring hybrids have been developed. They allow the design of arbitrary power division, arbitrary termination impedances, and especially small-sized ring hybrids. On the basis of these derived equations, a theoretical evaluation was made using microstrip ring hybrids, and experiments are demonstrated using a coplanar ring hybrid.**

***Index Terms*—Arbitrary power division, arbitrary termination impedances, power divider, ring coupler.**

I. Introduction

ALTHOUGH considered as narrow-banded devices, the rat-race hybrids (ring hybrids) and branch-line hybrids have been found in extensive applications of microwave circuits. Ring hybrids have a definite advantage over the branch-line hybrids in applications, e.g., antenna arrays, mixers, or balancing amplifiers, because no phase-compensation element is necessary. Ring hybrids have wider bandwidths than those of branch-line hybrids as well. In practical cases, hybrids can be used together with other devices. In that case, to obtain desired performances, additional matching networks are necessary.

If hybrids are terminated by arbitrary impedances, there is a big advantage to reduced circuit size. Since 1947, ring hybrids have been studied [1]–[3], but these studies focus on symmetrical-structure ring hybrids. Recently, for the first time, Ahn *et al.* treated an asymmetrical-structure ring hybrid for monolithic-microwave integrated-circuit (MMIC) application [4]. However, it is limited to equal-power split-ring hybrids.

Since Pon, several authors dealt with ring hybrids [5], [6] for arbitrary power division, but all of these analyses were applied to only symmetric structures (even- and odd-mode analyses) and the procedures to find out the correct characteristic impedances are somewhat complex.

In this paper, design equations for ring hybrids with both arbitrary termination impedances and arbitrary power division ratios will be described. The methods used for their derivation are quite different from the conventional ones. Also, design equations, which can be used in the case where the arc lengths are less than $\lambda/4$, have been developed. Again, these design equations can be used for ring hybrids with both arbitrary power division and arbitrary termination impedances.

On the basis of the derived design equations, a microstrip ring hybrid terminated by impedances 50, 45, 42, and 60 Ω, with a power split ratio of 4 dB, and four arcs of 75° electrical length was analyzed. As another example, a coplanar ring hybrid terminated by impedances 50, 45.45, 55.55, and 38.46 Ω, the same power split ratio of 4 dB, and four arcs of 75° electrical length was fabricated on coplanar strips (CPS's), CPS crossover, and coplanar waveguides (CPW's).

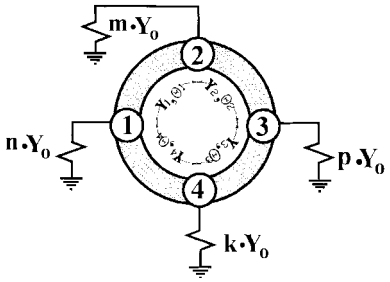

Fig. 1. Ring hybrid terminated by arbitrary impedances (with arbitrary power divisions).

II. Analyses

The general configuration of a ring hybrid is shown in Fig. 1.

In the case of conventional ring hybrids: n, m, p, and k, which describe termination impedances, are equal; the transmission line characteristic admittances Y_1, Y_2, Y_3, and Y_4 are of same value or two of them are equal; as there are symmetry planes in the ring structure, even- and odd-mode analyses are possible [1]–[3], [5]–[8]; and to find out design equations is somewhat complex.

In the case of the ring hybrid terminated by arbitrary impedances: n, m, p, and k are different from each other; transmission line characteristic admittances Y_1, Y_2, Y_3, and Y_4 are different from each other; and there is no symmetric plane: even- and odd-mode analyses are impossible.

For the conventional ring hybrid shown in Fig. 1, it is well understood that the excited power at port ① is split between port ② and port ④, while port ③ is isolated. This operation can be regarded as a power divider. For the

Manuscript received March 27, 1997; revised July 30, 1997. This work was supported by Duisburg University, under SFB 254.

H.-R. Ahn and I. Wolff are with the Department of Electrical Engineering, Gerhard Mercator University Duisburg, 47057 Duisburg, Germany.

I.-S. Chang is with the Department of Electronic Engineering, Sogang University, Seoul, Korea.

Publisher Item Identifier S 0018-9480(97)08338-5.

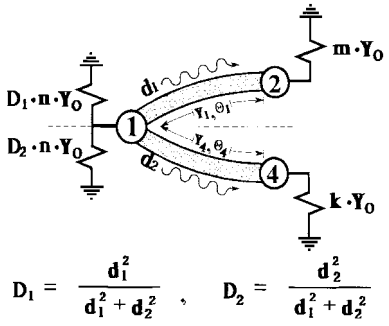

Fig. 2. The excitation of port ①.

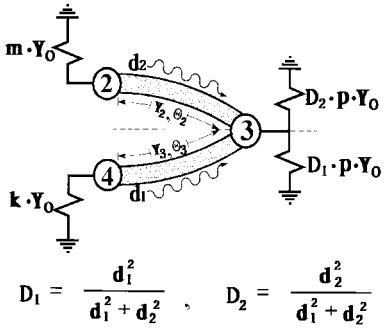

Fig. 3. The excitation of port ③.

excitation at port ③, similar arguments lead to an operation as a conventional power divider, except for an 180° difference between the two output arms.

The ring hybrid can be described by a four-port set of S-parameters given by

$$\begin{bmatrix} b_1 \\ b_2 \\ b_3 \\ b_4 \end{bmatrix} = \begin{bmatrix} S_{11} & S_{12} & S_{13} & S_{14} \\ S_{21} & S_{22} & S_{23} & S_{24} \\ S_{31} & S_{32} & S_{33} & S_{34} \\ S_{41} & S_{42} & S_{43} & S_{44} \end{bmatrix} \begin{bmatrix} a_1 \\ a_2 \\ a_3 \\ a_4 \end{bmatrix} \tag{1}$$

where $[\vec{b}]$ is the reflected power wave vector and $[\vec{a}]$ is the incident power wave vector. If port ③ is terminated by a reflection coefficient Γ_3, (1) can be expressed by

$$\begin{bmatrix} \vec{b}_1 \\ \vec{b}_2 \end{bmatrix} = \begin{bmatrix} \vec{S}_{11} & \vec{S}_{12} \\ \vec{S}_{21} & \vec{S}_{22} \end{bmatrix} \begin{bmatrix} \vec{a}_1 \\ \vec{a}_2 \end{bmatrix} \tag{2}$$

where

$$[\vec{b}_1] = \begin{bmatrix} b_1 \\ b_2 \\ b_4 \end{bmatrix} \quad [\vec{a}_1] = \begin{bmatrix} a_1 \\ a_2 \\ a_4 \end{bmatrix}$$
$$[\vec{b}_2] = [b_3] = \Gamma_3^{-1}[a_3] = [\vec{\Gamma}_2^{-1}][\vec{a}_2].$$

A straightforward calculation derives

$$[\vec{b}_1] = [\vec{S}_{11}][\vec{a}_1] + [\vec{S}_{12}][\vec{U} - \Gamma_3\vec{S}_{22}]^{-1}\Gamma_3[\vec{S}_{21}][\vec{a}_1]. \tag{3}$$

For the excitation at port ①, (3) can also be rewritten as

$$\begin{bmatrix} b_1 \\ b_2 \\ b_4 \end{bmatrix} = \begin{bmatrix} S_{11} & S_{12} & S_{14} \\ S_{21} & S_{22} & S_{24} \\ S_{41} & S_{42} & S_{44} \end{bmatrix} \begin{bmatrix} a_1 \\ 0 \\ 0 \end{bmatrix} + \frac{S_{31}a_1\Gamma_3}{1 - \Gamma_3 S_{33}} \begin{bmatrix} S_{13} \\ S_{23} \\ S_{33} \end{bmatrix}. \tag{4}$$

If $|S_{31}| = 0$ is assumed, (4) indicates that there is no correlation with Γ_3 in terms of port-① excitation. So under the condition of $|S_{31}| = 0$, the port-① excitation can be interpreted as shown in Fig. 2.

If the ring hybrid is lossless and passive, the S-parameters must satisfy the unitary condition

$$[\vec{S}][\vec{S}]^{*T} = [\vec{U}]. \tag{5}$$

Therefore, if the output arms are isolated from each other, and the input impedances are matched looking into any arm (when the other arms are terminated by matched impedances), (5) gives in detail

$$\begin{aligned} |S_{21}|^2 + |S_{41}|^2 &= 1 \\ |S_{12}|^2 + |S_{32}|^2 &= 1 \\ |S_{23}|^2 + |S_{43}|^2 &= 1 \\ |S_{14}|^2 + |S_{34}|^2 &= 1. \end{aligned} \tag{6}$$

A power split ratio is proportional to the square of the admittance ratio of the two variable admittances in the ring [5], [6]. Therefore, if the ratio, $|S_{21}| : |S_{41}|$ is $d_1 : d_2$, as in Fig. 2, the termination impedances of port ① can be divided as shown in Fig. 2, depending on the power delivered to port ② and port ④. If each length of the two arcs in Fig. 2 is $\lambda/4$, the characteristic admittances are

$$\begin{aligned} Y_1 &= \sqrt{mn}\sqrt{\frac{d_1^2}{(d_1^2 + d_2^2)}}\,Y_0 \\ Y_4 &= \sqrt{kn}\sqrt{\frac{d_2^2}{(d_1^2 + d_2^2)}}\,Y_0. \end{aligned} \tag{7}$$

In (7), m, n, p, and k are constants determined by the termination impedances. d_1 and d_2 are calculated according to a needed power division. Under the assumption of $|S_{31}| = 0$, the characteristic admittances Y_1 and Y_4 can be derived.

In case of a Y-junction, such as a Wilkinson power divider, an isolation resistor is needed [9]. Instead of the isolation resistor, for the ring hybrid shown in Fig. 1, the dummy arms of admittances Y_2 and Y_3 are connected with the two output ports ② and ④ to get these two ports isolated (in case of port- ① excitation). Therefore, the total power transferred to port ② can be delivered to the load at port ②. If the isolation is not ideal, an extremely small amount of power flows forward to port ③. Likewise, the total power reached at port ④ can be delivered to the load at port ④ and only an extremely small amount of power flows forward to port ③. For these two waves at port ③ to be isolated from port ①, two conditions must be satisfied: the waves must have a phase shift of 180° against each other, and the wave ratio must be $d_2 : d_1$, as shown in Fig. 3.

The above-mentioned second condition can be satisfied by (5) and (6). Also, as each length of the two arcs (Y_1, Y_4) is $\lambda/4$, one of the two remainder arcs (Y_2, Y_3) must be $\lambda/4$, and the other one $3\lambda/4$ long, to satisfy the first condition. Due to the reciprocity, we can also consider this circuit as being

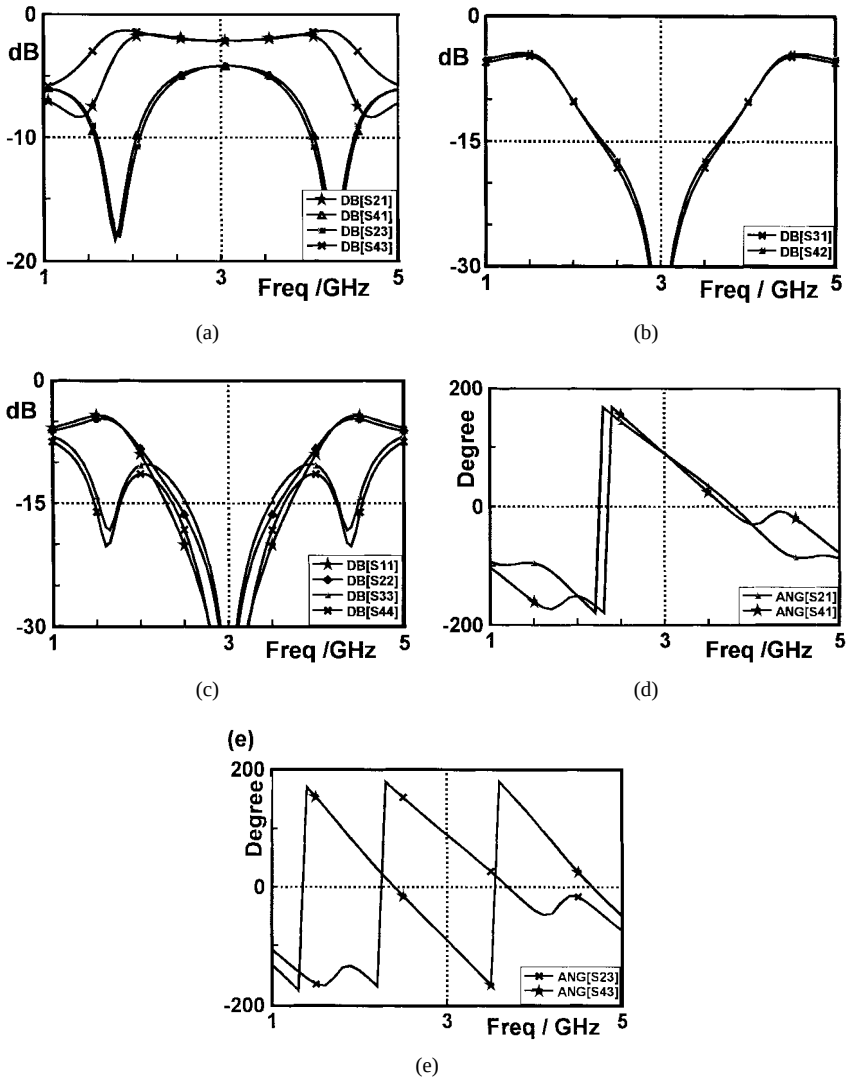

Fig. 4. Simulation results for $n = 1$, $m = 1.1$, $p = 0.7$, and $k = 0.8$, power split ratio = 2 dB. (a) $[S]$-parameters for power division, (b) $[S]$-parameters for isolation, (c) $[S]$-parameters for matching, (d) phases of S_{21} and S_{41}, and (e) phases of S_{23} and S_{43}.

excited at port ③ and the arms (Y_2, Y_3), which were removed in Fig. 2, can be shown as in Fig. 3. So the characteristic admittances are

$$Y_2 = \sqrt{mp}\sqrt{\frac{d_2^2}{(d_1^2+d_2^2)}}\,Y_0$$
$$Y_3 = \sqrt{kp}\sqrt{\frac{d_1^2}{(d_1^2+d_2^2)}}\,Y_0. \tag{8}$$

From (7) and (8), in case of $m = n = p = k$, the same results as given by Pon [5] are derived. If $d_1 : d_2 = 1 : 1$, the results are in agreement with those of Ahn *et al.* [4]. For $m = n = p = k$ and, additionally, $d_1 : d_2 = 1 : 1$, the admittances for the well-known 3-dB ring hybrid are found.

On the basis of the derived design equations, a simulation for the example $n = 1$, $m = 1.1$, $p = 0.7$, and $k = 0.8$, and a power split ratio of 2 dB (which means $20^* \log(d_1/d_2) = 2$ dB) was performed. For the analyses of the resulting ring hybrid, EEsof Libra was used as a simulator. The simulation results in Fig. 4(a) show that the power ratio is really 2 dB with $|S_{21}| = -2.124$ dB, $|S_{41}| = -4.124$ dB, $|S_{43}| = -2.124$ dB, and $|S_{23}| = -4.124$ dB. The simulation results for a lossless ring hybrid in Fig. 4(b) show that the power at the isolated ports ($|S_{31}| = -158.656$ dB and $|S_{42}| = -160.656$ dB) are theoretically zero at center frequency. All input reflection coefficients are shown in Fig. 4(c). The phase performances between two output arms are shown in Fig. 4(d) and (e). The value $|S_{21}| = -2.124$ dB can be obtained by $10^* \log^* [d_1^2/(d_1^2 + d_2^2)]$.

III. Small-Sized Ring Hybrid

The voltages in the two output arms are either in phase or 180° out of phase, depending on the input arms chosen. Conventional ring hybrids use arc lengths of $\lambda/4$ or $3\lambda/4$. To reduce the ring hybrid's size, lengths of $\lambda/8$ or $\lambda/6$ may be used [10]. Other approaches include the application of $\lambda/6$ or $\lambda/5$ arc lengths [11], [12]. In any case, three arcs of a ring are of equal length and the other one must provide a $\pm 180°$ phase shift compared to the three other ones. If the arc lengths are not $\lambda/4$ or $3\lambda/4$, the characteristic impedances are changed in proportion to the arc lengths [11], [12]. Thus, the characteristic

TABLE I
$n = 1$, $m = 1.1$, $p = 0.7$, AND $k = 0.8$,
$\Theta_1 = \Theta_2 = \Theta_4 = 80°$, $\Theta_3 = 180° + \Theta_1$, $Y_o = 1/50$ S

power split	matching	isolation	power division
0 dB	S_{11} = -49.37		S_{21} = -3.013
	S_{22} = -32.59	S_{31} = -40.4	S_{41} = -3.009
	S_{33} = -31.69	S_{24} = -38.4	S_{23} = -3.014
	S_{44} = -44.82		S_{43} = -3.013
2 dB	S_{11} = -44.14		S_{21} = -2.126
	S_{22} = -34.03	S_{31} = -41.9	S_{41} = -4.123
	S_{33} = -32.83	S_{24} = -39.6	S_{23} = -4.127
	S_{44} = -41.10		S_{43} = -2.127
4 dB	S_{11} = -41.30		S_{21} = -1.457
	S_{22} = -35.37	S_{31} = -44.0	S_{41} = -5.454
	S_{33} = -33.97	S_{24} = -41.5	S_{23} = -5.458
	S_{44} = -39.15		S_{43} = -1.457

admittances can be derived as

$$Y_1 = \sqrt{mn}\sqrt{\frac{d_1^2}{(d_1^2+d_2^2)(1-\cot^2\Theta_1)}}\,Y_0$$
$$Y_2 = \sqrt{mp}\sqrt{\frac{d_2^2}{(d_1^2+d_2^2)(1-\cot^2\Theta_2)}}\,Y_0$$
$$Y_3 = \sqrt{kp}\sqrt{\frac{d_1^2}{(d_1^2+d_2^2)(1-\cot^2\Theta_3)}}\,Y_0$$
$$Y_4 = \sqrt{kn}\sqrt{\frac{d_2^2}{(d_1^2+d_2^2)(1-\cot^2\Theta_4)}}\,Y_0. \qquad (9)$$

From (9), if $m = n = p = k$, $\Theta_1 = \Theta_4 = \Theta_2 = \lambda/6$, $\Theta_3 = 4\lambda/6$, and $d_1 : d_2 = 1 : 1$, the results are the same as those of [10]. If $m = n = p = k$, $d_1 : d_2 = 1 : 1$, and for general arc lengths, the results are also those of [11], [12].

Table I shows the simulation results of the scattering parameters of a ring hybrid at center frequency (3 GHz) on the basis of (9). All values in Table I are in decibels and n, m, p, and k are constants, which can be decided by the choice of the termination impedances in Fig. 1.

IV. WIDE-BANDWIDTH AND SMALL-SIZED RING HYBRIDS

A. Microstrip Ring Hybrid

The limiting factor in the conventional transmission-line ring hybrid is that the $180° + \Theta$ arc, which produces an 180° out-of-phase signal against the other Θ arcs, is just as effective in the vicinity of the center frequency of interest. To overcome this problem, for the first time, the wide-band ring hybrid using a set of shorted coupled transmission lines was realized in stripline technology. It operates with equal power splitting, equal termination impedances, and each electric arc length of 90° [13]. In this paper, analyses of a microstrip ring hybrid will be carried out at the frequency of 3 GHz using (9). This ring hybrid is terminated by the arbitrary impedances referred to in Table II, power split ratio of 4 dB and all-electrical arc lengths of the ring are 75°.

TABLE II
$n = 1$, $m = 1.11\cdots$, $p = 1.190$, AND $k = 0.833\cdots$,
$\Theta_1 = \Theta_2 = \Theta_3 = \Theta_4 = 75°$, $Y_o = 1/50$ S

Termination impedances	MS feeding transformer lines (μm)	MS ring transmission lines (μm)
port ①; 50 Ω	Z_{o1}; w = 609.7, l = 7935	Z_1; w = 520.4, l = 8071
port ②; 45 Ω	Z_{o2}; w = 677.0, l = 7895	Z_2; w = 297.7, s = 32, l = 8048
port ③; 42 Ω	Z_{o3}; w = 724.0, l = 7868	Z_3; w = 432.9, l = 8067
port ④; 60 Ω	Z_{o4}; w = 503.0, l = 8005	Z_4; w = 88.36, l = 8371

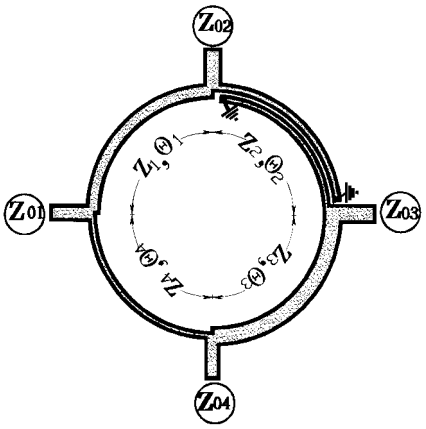

Fig. 5. Microstrip ring hybrid configuration.

Fig. 5 shows the microstrip ring hybrid according to the data specified in Table II. To realize a set of coupled transmission lines, Z_{oe} (even-mode impedance) and Z_{oo} (odd-mode impedance) must be given. The image impedance of a set of shorted coupled transmission lines was given by [14]

$$Z_I = \frac{2Z_{oe}Z_{oo}\sin\Theta}{[(Z_{oe}-Z_{oo})^2 - (Z_{oe}-Z_{oo})^2\cos^2\Theta]^{1/2}}. \qquad (10)$$

The coupling coefficient of coupled transmission lines is known as [15]

$$C_{\text{eff}} = \left|\frac{j[(Z_{oe}/Z_{oo})^{0.5} - (Z_{oe}/Z_{oo})^{-0.5}]\sin\Theta}{D_{\text{eff}}}\right|$$

where

$$D_{\text{eff}} = 2\cos\Theta + j[(Z_{oe}/Z_{oo})^{0.5} + (Z_{oe}/Z_{oo})^{-0.5}]\sin\Theta. \qquad (11)$$

Any section of the ring can be substituted by a set of shorted coupled transmission lines. Depending on the coupling coefficients, the Z_{oe} and Z_{oo} of each arc can be calculated using (10) and (11), as shown in Table III. All values in Table III are in Ω.

The big problem of this ring hybrid is how to fabricate the parallel coupled lines with 3-dB coupling [16]. Fig. 6

TABLE III
$Z_1 = 54.0\ \Omega$, $Z_2 = 78.5\ \Omega$, $Z_3 = 57.2\ \Omega$, $Z_4 = 98.9\ \Omega$, AND $\Theta_1 = \Theta_2 = \Theta_3 = \Theta_4 = 75°$

	Z_{oe}	Z_{oo}	Z_{oe}	Z_{oo}	Z_{oe}	Z_{oo}	Z_{oe}	Z_{oo}
Z_1	134.3	21.8	111.5	21	92.7	20.1	67.8	18.3
Z_2	195.1	31.7	160.5	30.45	134.7	29.2	98.5	26.5
Z_3	142.1	23.1	117	22.2	98.1	21.2	71.8	19.3
Z_4	254	40	202	38.4	169.7	36.7	124	33.4

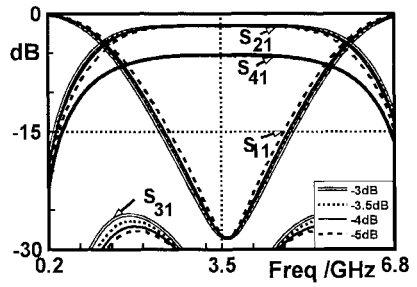

(a)

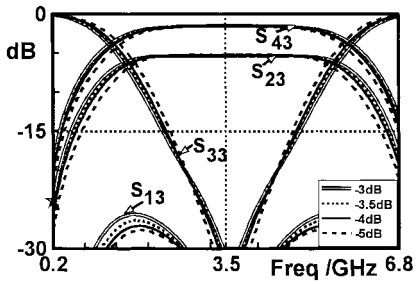

(b)

Fig. 6. The simulation results for a microstrip ring hybrid terminated by 50, 45, 42, and 60 Ω, power split ratio, 4 dB, lengths of the four arcs, 75°. (a) Port-① excitation. (b) Port-③ excitation.

shows simulation performances depending on the coupling coefficient. For its simulations, all elements are used with physical realizable values, except one set of shorted coupled transmission lines between ports ② and ③, as shown in Fig. 5. Fig. 6(a) and (b) show wide-band ring hybrid performances. Again, coupling coefficients are different from each other; nevertheless, output results are about the same in band, i.e., as the realization of 3-dB coupled transmission lines with microstrip technology is seen as not so easy, to get wide-band microstrip ring hybrids instead of 3-dB coupled transmission lines, 4- or 5-dB coupled transmission lines can be used. This fact was also proven by [4]. The experimental data of the ring hybrid on Al_2O_3 substrate ($\varepsilon_r = 10$ and $h = 635\ \mu$m), including a set of shorted coupled lines marked in Table III, are given in Table II.

B. Uniplanar Ring Hybrid

Another approach to realize constant 180° phase shift ring hybrids has been demonstrated in coplanar technology [11], [12], [16], [17]. All these are limited to equal power division and equal termination impedances. In this paper, an experiment

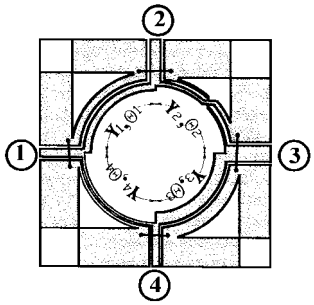

Fig. 7. The configuration of a ring hybrid in coplanar technology.

TABLE IV
$n = 1$, $m = 1.1$, $p = 1.3$, AND $k = 0.9$, $\Theta_1 = \Theta_2 = \Theta_3 = \Theta_4 = 75°$, $Y_o = 1/50$ S

Termination impedances	Transmission line admittances	CPS physical size (μm)
port ①; 50 Ω	Y_1; 0.0184 S	Y_1; w = 700, s = 47
port ②; 45.45 Ω	Y_2; 0.0132 S	Y_2; w = 300, s = 94
port ③; 38.46 Ω	Y_3; 0.0187 S	Y_3; w = 1000, s = 52
port ④; 55.56 Ω	Y_4; 0.0105 S	Y_4; w = 120 , s = 89

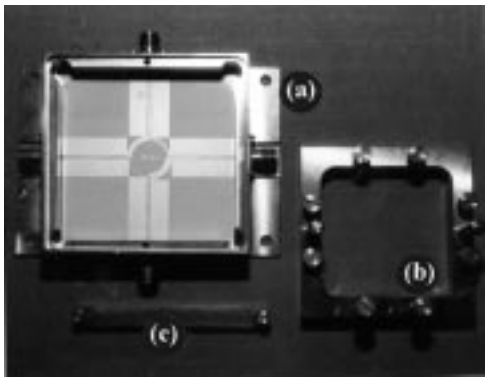

Fig. 8. The package used for the coplanar measurement.

was done using the circuit proposed by [11]. Fig. 7 shows a coplanar ring hybrid. Its termination impedances and the length of the arcs are shown in Table IV. The power split ratio is 4 dB and the center frequency f_o is 3 GHz. Also, its experimental data on Al_2O_3 substrate ($\varepsilon_r = 10$ and $h = 635\ \mu$m) are shown in Table IV.

This ring hybrid is not terminated by 50 Ω. Thus, additional transformers are necessary in the measurement. Due to the large-sized circuit, on-wafer measurement cannot be carried out. There are special connectors for larger-sized coplanar circuits, but these are available only for two-port circuits. Therefore, a special package for a four-port coplanar ring hybrid is indispensable. Fig. 8 shows the package used for measurement.

As shown in Fig. 8, in principle, as coplanar circuits require no backside metallization, the space between the substrate and the bottom of the package (a) is filled with air. Also, a package (b) is needed for providing good contact between the walls of the package (a) and the ground planes of the CPW's. An

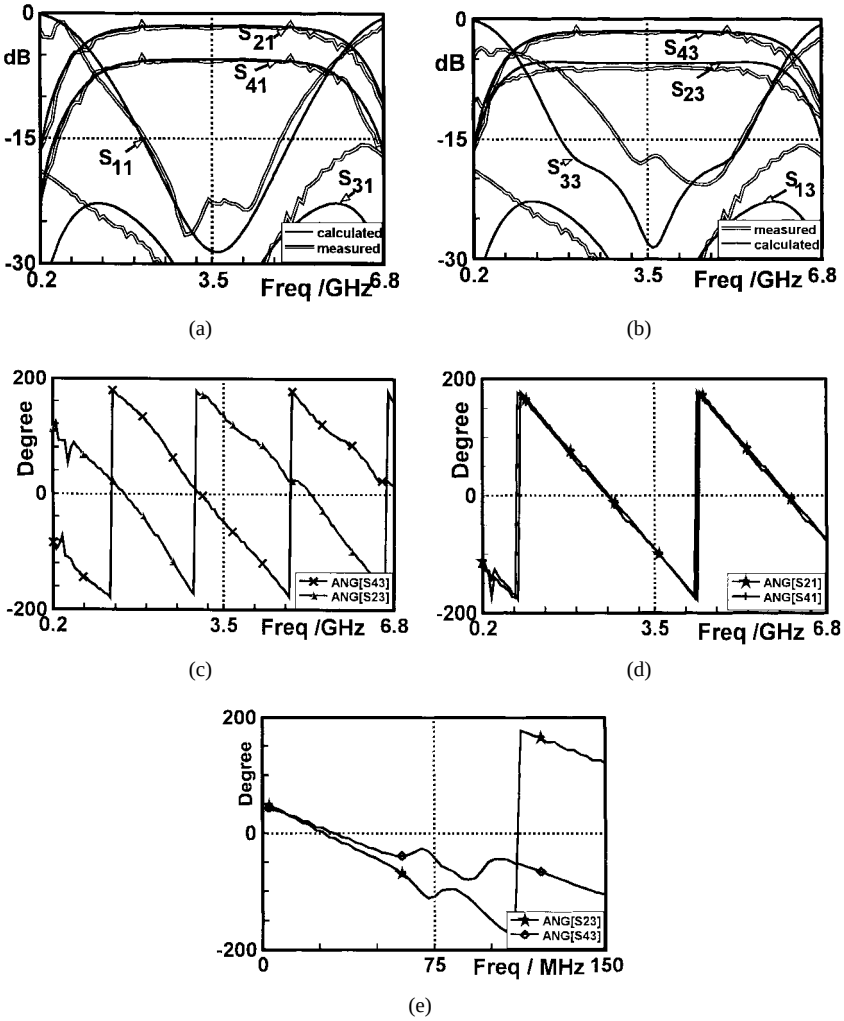

Fig. 9. Measured and calculated responses of a coplanar ring hybrid terminated by arbitrary impedances, 50, 45.45, 55.55, and 38.46 Ω, power split ratio of 4 dB, 4 arcs of 75° electrical length. (a) Measured and calculated $[S]$-parameters (in case of port-① excitation), (b) measured and calculated $[S]$-parameters (in case of port-③ excitation), (c) measured phase responses of S_{23} and S_{43}, (d) measured phase responses of S_{23} and S_{43}, (e) measured phase responses of S_{23} and S_{43} (in low frequency range).

additional bar (c) is necessary to make the circuit stable during measuring.

Fig. 9 shows comparisons between calculated and measured results. Fig. 9(a) shows the magnitude of the scattering parameters of the ring hybrid for excitation at port ①, and Fig. 9(b) shows the excitation at port ③. Fig. 9(c)–(e) depicts the phases of the scattering parameters. The deviations between simulation and experimental results for $|S_{33}|$ in Fig. 9(b) are due to unexpected stray inductances in the course of line crossover (see Fig. 7). Nevertheless, the results for port-① excitation show good performance, which proves (4). Finally, Fig. 9(e) shows the change of the phases of S_{23} and S_{43} with increasing frequency. As frequency goes up to 150 MHz, it shows that the difference between S_{23} and S_{43} in phases goes to 180° in Fig. 9(e).

V. Conclusion

In this paper, new design equations for ring hybrids terminated by arbitrary impedances are presented. These design equations show that they can be applied in any case of arbitrary power division, arbitrary length of the arcs, and arbitrary termination impedances. Using this design method, there are large advantages gained by reducing the total size of integrated microwave circuits.

References

[1] W. A. Tyrrel, "Hybrid circuits for microwaves," *Proc. IRE,* vol. 35, pp. 1294–1306, Nov. 1947.
[2] L. Young, "Branch guide directional couplers," presented at the *Proc. Nat. Electron. Conf.,* Chicago, IL, Oct. 1956.
[3] J. Reed and G. J. Wheeler, "A method of analysis of symmetrical four-port networks," *IRE Trans. Microwave Theory Tech.,* vol. MTT-4, pp. 346–352, Oct. 1956.
[4] H.-R. Ahn, I.-S. Chang, and S. W. Yun, "Miniaturized 3-dB ring hybrid terminated by arbitrary impedances," *IEEE Trans. Microwave Theory Tech.,* vol. 42, pp. 2216–2221, Dec. 1994.
[5] C. Y. Pon, "Hybrid-ring directional coupler for arbitrary power divisions," *IRE Trans. Microwave Theory Tech.,* vol. MTT-9, pp. 529–535, Nov. 1961.
[6] A. K. Agrawal and G. F. Mikucki, "A printed circuit hybrid ring directional coupler for arbitrary power division," *IEEE Trans. Microwave Theory Tech.,* vol. MTT-34, pp. 1401–1407, Dec. 1986.
[7] G. F. Mikucki and A. K. Agrawal, "A broad-band printed circuit hybrid ring power divider," *IEEE Trans. Microwave Theory Tech.,* vol. 37, pp. 112–117, Jan. 1989.
[8] D. Kim and Y. Natio, "Broad-band design of improved hybrid-ring 3-dB directional coupler," *IEEE Trans. Microwave Theory Tech.,* vol.

MTT-30, pp. 2040–2046, Nov. 1982.
[9] N. Nagai, E. Maekawa, and K. Ono, "New n-way hybrid power dividers," *IEEE Trans. Microwave Theory Tech.*, vol. MTT-25, pp. 1008–1011, Dec. 1977.
[10] D. I. Kim and G. S. Yang, "Design of a new hybrid-ring directional coupler using $\lambda/8$ or $\lambda/6$ sections," *IEEE Trans. Microwave Theory Tech.*, vol. 39, pp. 1179–1783, Oct. 1991.
[11] B.-H. Murgulescu, E. Moisan, P. Legaud, E. Penard, and I. Zaquine, "New wideband, 0.67 λg circumference 180° hybrid ring coupler," *Electronic Lett.*, vol. 30, no. 4, pp. 299–300, Feb. 1994.
[12] L. Fan, C.-H. Ho, S. Kanamaluru, and Kai-Chang, "Wide-band reduced sized uniplanar magic-T, hybrid ring, and de Ronde's CPW-slot couplers," *IEEE Trans. Microwave Theory Tech.*, vol. 43, pp. 2749–2758, Dec. 1995.
[13] S. Mar, "Wideband stripline hybrid ring," *IEEE Trans. Microwave Theory Tech.*, vol. MTT-16, pp. 361–362, June 1968.
[14] E. M. T. Jones and J. T. Bolljahn, "Coupled-strip transmission-line filters and directional couplers," *IRE Trans. Microwave Theory Tech.*, vol. MTT-4, no. 2, pp. 75–81, Apr. 1956.
[15] P. Bhartia and I. J. Bhal, *Millimeter Wave Engineering and Applications.* New York: Wiley, 1984, pp. 373–374.
[16] C.-H. Ho, L. Fan, and K. Chang, "Broad-band uniplanar hybrid-ring and branch-line couplers," *IEEE Trans. Microwave Theory Tech.*, vol. 41, pp. 2116–2124, Dec. 1993.
[17] ———, "New uniplanar coplanar waveguide hybrid-ring couplers and magic-T's," *IEEE Trans. Microwave Theory Tech.*, vol. 42, pp. 2440–2448, Dec. 1994.

Hee-Ran Ahn (S'94–M'97) received the B.S., M.S., and Ph.D. degrees, all in electronic engineering, from Sogang University, Seoul, Korea, in 1988, 1990, and 1994, respectively.

From 1991 to 1995, she was a Part-Time Lecturer at Sogang University. Since 1996, she has been a Post-Doctoral Fellow with the faculty of electromagnetic-field theory, Department of Electronic Engineering, Duisburg University, Duisburg, Germany, where she works on a 60-GHz receiver as a part of SFB 254. Her current interests include high-frequency circuit design.

Ingo Wolff (M'75–SM'85–F'88) was born on September 27, 1938, in Köslin, Germany. He studied electrical engineering from 1958 to 1964, and received the Dipl.-Ing. Dr.-Ing. degrees, and the habilitation degree in high-frequency techniques and technologies from the Technical University Aachen, Germany, in 1964, 1967, and 1970, respectively.

In 1974, he took over as Chair of Electromagnetic Field Theory, Duisburg University, Duisburg, Germany. In addition to this position, he is currently a Professor. In 1992, he founded the Institute of Mobile and Satellite Communication Techniques, Kamp-Lintfort, Germany, which is a research institute for radio communication techniques, where he is currently the Managing Director.

Ik-Soo Chang (M'79) received the B.S., M.S., and Ph.D. degrees, all in electronic engineering, from Seoul National University, Seoul, Korea, in 1968, 1970, and 1979, respectively. From 1969 to 1971, he worked in the Research Center of the Korean Ministry of Communication. From 1971 to 1974, he served in the military as a Full-Time Instructor at the Korean Military Academy. Since 1974, he has been a Professor with the Department of Electronic Engineering, Sogang University, Seoul, Korea. From September 1982 to August 1983, he was a Visiting Professor at the University of Wisconsin–Madison. His principal research is RF circuit design.